

# Kinome analyses of inflammatory responses to swine barn dust extract in human bronchial epithelial and monocyte cell lines

Sabari Nath Neerukonda<sup>1</sup> , Sanjana Mahadev-Bhat<sup>2</sup>,  
Bridget Aylward<sup>1</sup>, Casey Johnson<sup>1</sup>,  
Chandrashekhar Charavaryamath<sup>2,\*</sup> and Ryan J Arsenault<sup>1,\*</sup> 

*Innate Immunity*  
2018, Vol. 24(6) 366–381  
© The Author(s) 2018  
Article reuse guidelines:  
sagepub.com/journals-permissions  
DOI: 10.1177/1753425918792070  
journals.sagepub.com/home/ini



## Abstract

Exacerbated inflammation upon persistent barn organic dust exposure is a key contributor to the pathogenesis of lung inflammation and lung function decline. Barn dust constituents and the mechanisms contributing to the exacerbated inflammation are not clearly known. We set out to understand the inflammatory effects of Swine Barn Dust Extracts (SBDE) on human lung epithelial (BEAS2B) and macrophage (THP-1 monocyte derived) cell lines on a kinome array to determine phosphorylation events in the inflammatory signaling pathways. Upon identifying events unique to SBDE or those induced by innate immune ligands in each cell line, we validated the signaling pathway activation by transcriptional analyses of downstream inflammatory cytokines. Our findings indicate that SBDE-mediated pro-inflammatory effects are predominantly due to the induction of neutrophilic chemokine IL-8. Differentially phosphorylated peptides implicated in IL-8 induction in BEAS2B cell line include, TLR2, 4, 5, 7, 8, 9, PKC, MAP kinases (p38, JNK), inflammasomes (NLRP1, NLRP3), NF- $\kappa$ B and AP-1. In the THP-1 cell line, in addition to the aforementioned peptides, peptides corresponding to RIG-I-like receptors (RIG-I, MDA5) were found. This is the first report to demonstrate the application of a kinome array to delineate key inflammatory signaling pathways activated upon SBDE exposure *in vitro*.

## Keywords

Pro-inflammatory cytokines, kinome, swine barn dust, signaling, lung epithelial, monocyte

Date received: 3 June 2018; revised: 6 July 2018; accepted: 10 July 2018

## Introduction

Agricultural workers, including swine production workers, are at an increased risk for developing respiratory disorders such as rhinosinusitis, chronic bronchitis, and chronic obstructive pulmonary disease (COPD) accompanied with lung function decline.<sup>1</sup> This is due to an increase in concentrated animal feeding operations (CAFOs) that predispose the farmers working 8 h shifts and are exposed to significant amounts of airborne dust generated in the barns.<sup>1,2</sup> Repeated or chronic exposure of farmers to the barn dust enriched in microbial and non-microbial organic components is implicated in respiratory disease development; symptoms appear to be proportionate to the dust levels and dust reduction strategies have resulted in symptom reduction.<sup>3,4</sup>

Microbial components of the dust from swine farming facilities were found to comprise a large number (90%) of sequences pertaining to Gram-positive anaerobic bacteria and methanogenic Archaea upon shotgun pyrosequencing.<sup>5,6</sup> The top four genera in the swine facility dust were assignable to the *Clostridium*,

<sup>1</sup>Department of Animal and Food Sciences, University of Delaware, USA

<sup>2</sup>Department of Biomedical Sciences, College of Veterinary Medicine, Iowa State University, USA

\*These authors contributed equally to the work.

### Corresponding author:

Ryan J Arsenault, Department of Animal and Food Sciences, University of Delaware, 022 Townsend Hall 531 South College Ave, Newark, DE 19716, USA.  
Email: rja@udel.edu.



*Lactobacillus*, *Ruminococcus*, and *Eubacterium* species.<sup>7</sup> In addition, gas chromatography combined with MS analysis of settled swine barn dust revealed the presence of high amounts of muramic acid, a peptidoglycan (PGN) component present mainly in Gram-positive bacteria.<sup>8</sup> In addition, fungal  $\beta$ -glucans were also present and were implicated in the modulation of agricultural dust-induced inflammation.<sup>8</sup> Although endotoxin, a cell envelope component of Gram-negative bacteria, is present in significant amounts in barn dusts and is linked to barn dust-induced airway inflammation, a considerable amount of research attributes a very minor to no role to endotoxin in contributing to airway inflammation.<sup>9-11</sup>

Airway inflammation upon exposure to barn dust occurs in response to recognition of microbial components or PAMPs present in the barn dust by PRRs. These PRRs are present in the interior cell compartments or exterior cell surface. Three main families of PRRs present in the cell include; TLRs, retinoic acid inducible gene-I like receptors (RLRs), and NLRs. Among TLRs, TLR4 forms a complex with CD14 and MD2, and recognizes bacterial LPS presented via LPS binding protein (LBP), resulting in the downstream activation of adaptors (MyD88 and TRIF) and a cascade of kinases, ultimately leading to transcriptional induction of pro-inflammatory cytokines (IL-1 $\beta$ , IL-6, IL-8, TNF- $\alpha$ ) and relatively less Type I IFNs (IFN- $\beta$ , - $\alpha$ ). Studies delineating the role of TLR4 in swine barn air-induced lung dysfunction in wild type (WT) and TLR4 mutant mice have implicated TLR4 independent mechanisms responsible for airway inflammation upon chronic exposure to swine barn dust air.<sup>2</sup> Studies using endotoxin-depleted barn dust samples have elicited inflammatory responses in a variety of cells to indicate inflammatory potential of components other than endotoxin in the dust samples.<sup>12-14</sup> Following exposure to swine barn dust extract, airway epithelial cells up-regulated TLR2 mRNA and protein in a concentration-dependent manner and specific Ab-mediated blocking of TLR2 dampened the pro-inflammatory cytokine release *in vitro*.<sup>15,16</sup> In a TLR2-deficient mouse model, single and repeated exposures to swine barn dust resulted in a significant reduction in neutrophil influx, cytokine production and loss of lung parenchyma was observed. However, airway hyper responsiveness (AHR) and NO release still persisted in these mice.<sup>17-19</sup> Finally, cytoplasmic NLR, NOD2, which recognizes muramyl dipeptide from Gram-positive bacterial cell wall is implicated in airway inflammation.<sup>20</sup> Taken together, these evidences indicate the complexity of host inflammatory response upon swine barn dust exposure.

Airway epithelial cells in general are the primary cells that interface respiratory tract to the environment and are the first responders to the constituents of dust extracts.<sup>21</sup> BEAS-2B or primary human bronchial

epithelial cells (HBEC) are the two frequently used cell types to model the responses to swine barn dust extracts (SBDE) *in vitro*.<sup>12,22</sup> SBDE exposure of either BEAS-2B or primary HBEC leads to production of IL-6, IL-8 and TNF- $\alpha$  in a PKC-dependent manner.<sup>22</sup> SBDE exposure leads to sequential activation of PKC isoforms with an early activation of PKC $\alpha$  isoform within 1 h post exposure to promote TNF- $\alpha$  and IL-6 production.<sup>23</sup> Apart from epithelial cells lining the respiratory tract, lung alveolar macrophages play a critical role in maintaining lung homeostasis by limiting the inflammation, at the same time functioning to promote defense towards respiratory pathogens. Monocytes, when differentiated into macrophages in the presence of endotoxin depleted organic dust extracts (ODE), a significant reduction in surface marker expression (HLA-DR, CD80, CD86), phagocytic activity and cytokine responsiveness was observed.<sup>24</sup> This differentiation model indicated that repeated exposure to organic dusts significantly impairs the normal function of monocyte-derived macrophages.<sup>24</sup> This impaired macrophage function was also observed in swine alveolar macrophages upon treatment with SBDE.<sup>25</sup> Furthermore, in swine macrophages an increase in porcine reproductive and respiratory syndrome virus (PRRSV) receptor CD163 was observed.

In the current study, inflammatory responses to SBDE treatment were modeled *in vitro* in two well-established human cell lines namely, BEAS-2B, a bronchial epithelial cell line<sup>26</sup> and THP-1, a human acute leukemic monocytic cell line established from a leukemic patient.<sup>27</sup> We chose these cell lines to represent airway epithelial (BEAS-2B) and resident or recruited alveolar macrophages (THP-1), since inhaled swine barn dust has been shown to induce airway epithelial as well as alveolar inflammation.<sup>28</sup> With the extensive existing knowledge of signaling event modifications occurring prior to and independent of changes in cellular transcription or translation, we took advantage of characterizing post translational modifications; in particular, kinase-mediated phosphorylation events. Using kinome peptide arrays, we characterized phosphorylation-mediated signal transduction events in BEAS-2B and THP-1 cell lines treated with SBDE or innate immune ligands LPS or PGN. We then compared SBDE-induced signaling pathways with those induced upon treatment with LPS and PGN. Upon comparison, unique or shared signaling pathways among treatments were identified and further validated by transcriptional analyses of downstream target genes using quantitative real time PCR. Finally, comparisons were made between the cell lines BEAS-2B and THP-1 in terms of magnitude of responses to SBDE. This comparison was made in order to implicate critical cell types responsible for airway inflammation and lung pathology. Although the cell types employed in the current

study are not primary cell types, they were frequently employed in past studies to investigate responses to barn dust, with no significant response variation observed when compared with primary cell types.<sup>14,18,20,22</sup>

## Materials and methods

### Cell culture

Prior to all experiments, live/dead cell count was determined by 4% trypan blue dye exclusion for viability. Cell populations with a minimum of 95% viability were used for the experiments. HBEC line (BEAS-2B, ATCC CRL-9609) was seeded ( $1 \times 10^6$ ) onto type I bovine collagen (StemCell Technologies, Vancouver, BC)-coated T-75 flasks. Cells were maintained in serum-free LHC-9 medium (Gibco) containing penicillin/streptomycin (100 U/ml; Gibco) and amphotericin B (2 µg/ml; Sigma) in a humidified chamber at 37°C/5% CO<sub>2</sub> until 80% confluent. Immortalized human monocytic cell line (THP-1, ATCC TIB-202) was maintained in suspension culture in Roswell Park Memorial Institute medium (RPMI-1640, Gibco) containing 10% of heat inactivated FBS (Atlanta Biologics) and supplemented with HEPES buffer (10 mM; Gibco), sodium pyruvate (1 mM; Sigma), D-Glc (4.5 g/l; Sigma), sodium bicarbonate (1.5 g/l; Sigma), penicillin/streptomycin (100 U/ml; Gibco) and amphotericin B (2 µg/ml; Sigma). Cells were maintained in a humidified chamber at 37°C/5% CO<sub>2</sub>.  $2-3 \times 10^6$  cells were stimulated with 10 nM phorbol 12-myristate 13-acetate (PMA, Sigma) diluted in RPMI-1640 with 1% FBS for 24 h to differentiate monocytes into macrophages and incubated for an additional 24 h.

### SBDE preparation

Settled dust was collected from commercial swine production units. Dust was brushed into zip lock bags containing a desiccant, transported to the laboratory on ice and stored at -80°C until processed. SBDE was prepared as previously described.<sup>22</sup> Briefly, dust collected was weighed and 1 g of the dust was placed in 10 ml of Hank's Balanced Salt Solution (HBSS) without calcium (Gibco). The mixture was vortexed and allowed to stand at room temperature for 1 h. The mixture was centrifuged for 20 min (1365 g, 4°C). Supernatant was collected, centrifuged again at 1365 g and 4°C. The final supernatant was collected, and filter sterilized by passing through a 0.22 µm filters (EMD Millipore). Filtered SBDE was aliquoted and stored at -80°C.

### Experimental treatments

SBDE, LPS (*Escherichia coli* O127:B8; Sigma), and PGN (*Staphylococcus aureus*; Sigma) treatments were

performed on BEAS-2B and THP-1 cell lines. Ligand stimulants (SBDE, LPS, PGN) were prepared by dissolving stock concentrations in a serum-free culture medium to achieve a final concentration of 10 µg/ml (LPS and PGN) and 5% (SBDE), respectively. Five percent SBDE is known to induce maximal pro-inflammatory response with limited cytotoxicity.<sup>13</sup> Stimulant treatments were performed at the respective final concentrations and media alone treated cells served as no treatment controls. Stimulant and no treatment control cell pellets were prepared at 0- and 24-h post treatment for kinome and transcriptional analyses.

### Kinome analyses

Kinome analyses was performed as previously described by Arsenault et al.<sup>29,30</sup> Briefly, cell lysates were prepared in 100 µl lysis buffer comprised of protease and phosphatase inhibitors followed by a 10 min incubation period on ice. After a brief centrifugation for 10 min, 70 µl supernatants were mixed with 10 µl of activation mix followed by incubation on the human peptide array slides at 37°C overnight. Slides were washed with 1% Triton - PBS, air dried and immersed in phospho-specific fluorescent ProQ Diamond Phosphoprotein Stain (Invitrogen) to agitate for 1 h. Slides were then washed three times in destaining solution containing 20% acetonitrile (EMD Biosciences, VWR Distributor, Mississauga, ON, Canada) and 50 mM sodium acetate (Sigma) at pH 4.0 for 10 min. A final wash was done with distilled deionized water. Slides were then air dried and briefly centrifuged at 300 g for 2 min to remove any residual moisture.

Array slides were read using a Tecan PowerScanner (TECAN Männedorf, Switzerland) at 532 to 560 nm with a 580-nm filter to detect dye fluorescence. Images were collected using GenePix, version 6.0, software (MDS), and spot intensity signal was collected as a mean of pixel intensity using local feature background intensity calculation with the default scanner saturation level. Differentially phosphorylated peptides in treatments relative to media alone treated control cells were determined.

### RNA extraction, cDNA synthesis and qRT-PCR analysis

RNA purification was performed from SBDE-, LPS- and PGN-treated cells with Qiagen RNeasy kit according to manufacturer's instructions (Qiagen Inc.). To avoid potential host chromosomal DNA contamination, RNA samples were treated with on-column DNase I (Qiagen Inc.). Total RNA quality (260/280 ratio) and quantity (at 260 nm absorbance) were measured using an Agilent Nanodrop spectrophotometer. cDNA synthesis was carried out with 500 ng RNA using the iScript Advanced cDNA synthesis kit

(Bio-Rad, CA) following manufacturer's instructions. Final cDNAs were diluted 10fold and 1  $\mu$ l of the diluted cDNA was used in a 20  $\mu$ l qPCR reaction consisting of 10  $\mu$ l iTaq Universal SYBR<sup>®</sup> Green Supermix (Bio-Rad, Hercules, CA), 8.2  $\mu$ l of nuclease free water and 0.4  $\mu$ l (250 nM) each of forward and reverse primers on a MyiQ2 Two-Color Real-Time PCR Detection System (Bio-Rad, Hercules, CA). Melt curve analysis was performed following PCR amplification to exclude non-specific amplification. Relative expression of target genes was based on normalization to endogenous reference gene GAPDH using the Relative Expression Software Tool (REST, Qiagen Inc.). Target gene selection bases and their primer sequences were mentioned in Supplementary data Tables 1, 2 and 3, respectively. Differences in gene expression levels between medium only control and treated samples were assessed in group means for statistical significance by pair wise fixed reallocation randomization test by REST software with a significance criteria of  $P < 0.05$ .<sup>31,32</sup>

#### Database for Annotation, Visualization and Integrated Discovery (DAVID) analysis

Differentially phosphorylated peptides and their corresponding UniprotKB entry ID lists ( $P \leq 0.05$ ) for each treatment were input and submitted to the gene list tab of DAVID with selected default background "*Homo sapiens*".<sup>33</sup> This is due to the fact that a larger gene background tends to produce smaller  $P$  values than prebuilt backgrounds on the chips, in our case arrays.<sup>33</sup> Gene Ontology (GO) term enrichments under the section "Functional annotation chart" and annotation term relationships among the proteins in the input list under the section "Functional annotation clustering" were downloaded in XML format. Upon functional annotation, KEGG pathways under the DAVID pathway viewer were explored for significantly enriched pathways related to innate immunity and are described in the results section.

#### Ingenuity Pathway Analysis (IPA)

The kinome data set which included UniprotKB entry identifiers (IDs), fold changes and  $P$  values for each

differentially phosphorylated peptide was input into IPA using the core analysis platform (Qiagen Inc.). The core analysis matched and retrieved proteins in our data set with those in the Ingenuity Knowledge Base, created molecular networks, divided the data set into biological functions that were significantly over represented and determined overrepresented canonical pathways. One hundred percent of input IDs were mapped to their corresponding proteins. Core analyses was performed with default settings: direct and indirect relationships between proteins supported by experimental treatments were considered, networks did not exceed 35 proteins, and all sources of data from human, mouse, and rat studies in the Ingenuity Knowledge Base were considered. Since the input IDs are selected based on their differential phosphorylation status and significance ( $P < 0.05$ ), no cut-offs were applied with regards to fold changes and  $P$  values. IPA generated priority lists for enriched molecular networks, biological functions, canonical pathways, differentially abundant proteins, and predicted upstream regulators. Network scoring was based on the number of mapped proteins in the network, network size, and the number of proteins in the Ingenuity Knowledge Base that could be included in the network. Network scores were calculated based from hypergeometric distribution and right-tailed Fisher's exact test.

## Results

### SBDE-induced kinome signaling in BEAS-2B cell line

In BEAS-2B cells treated with SBDE, significantly over-represented DAVID pathway clusters include chemokine signaling, pathways in cancer, TLR signaling pathways, TNF- $\alpha$  signaling pathway, and pathways associated with virus infections (Influenza A Virus (IAV), Hepatitis B Virus (HBV) and Hepatitis C Virus (HCV)) (Table 1). Among them, we intend to focus on relevant innate immune signaling pathways. To begin with, components in the SBDE are recognized by PRRs such as TLRs. Based on this, differential phosphorylation of TLR adaptor MyD88 was observed with subsequent downstream activation of kinases (IRAK1, IRAK4, I $\kappa$ BK- $\alpha$ , - $\beta$ , - $\epsilon$ ) that activate the

**Table 1.** DAVID GO-term enrichment of innate immune pathways in BEAS-2B cell line treatments.

SBDE	LPS	PGN
hsa04620: TLR signaling	hsa04620: TLR signaling	hsa04620: TLR signaling
hsa04668: TNF- $\alpha$ signaling	hsa04668: TNF- $\alpha$ signaling	hsa04062: Chemokine signaling
hsa04062: Chemokine signaling		hsa04668: TNF- $\alpha$ signaling
hsa04621: NLR signaling		
hsa04010: MAPK signaling		

DAVID: Database for Annotation, Visualization and Integrated Discovery.



**Table 2.** Differentially phosphorylated substrate peptides in SBDE-, LPS- and PGN-treated BEAS-2B cell line.

<sup>1</sup> Phosphoprotein	<sup>2</sup> Kinase target	SBDE		LPS		PGN	
		<sup>3</sup> Fold change	<sup>4</sup> P value	<sup>3</sup> Fold change	<sup>4</sup> P value	<sup>3</sup> Fold change	<sup>4</sup> P value
CXCR3	Y308	−1.10791	0	−1.18266	0.00495	−1.11545	0
IKBKA	T23	−1.06453	0.00007	−	−	−1.09075	0.00001
IKBKB	S181	−1.079	0.02114	−1.22367	0.03724	−1.09744	0.00202
IKBKE	S172	−1.03612	0.04982	−	−	−1.07972	0.00112
IKBKE	Y179	−1.09781	0.01142	−1.2448	0.02312	−1.08286	0.00111
IFNAR1	S535	1.27121	0.03298	1.24293	0.03082	1.25412	0.04089
IFNGR1	Y457	1.25248	0.02413	−	−	−	−
IRF3	S396	−1.09276	0	−1.05734	0.00236	−1.0913	0.00001
IRF5	S446	−1.0764	0.00406	−	−	−1.10525	0.00018
IRF7	S477	−1.09814	0.02072	−	−	−1.10052	0.00399
IFITM1	T73	−1.03791	0.03032	−	−	−1.05714	0.01192
IL-1R	Y496	−1.11188	0.03318	−1.47308	0.0129	−1.07836	0.00223
IL-1R	T210	−1.10114	0.0006	−1.32818	0.01251	−	−
IRAK1	T66	−1.07702	0.00274	−1.04005	0.00867	−1.08373	0.00136
IRAK1	T209	−1.1071	0.00043	−1.05067	0.00426	−1.09252	0.00056
IRAK1	T100	−1.14194	0.00017	−1.09488	0.00326	−1.12433	0.00145
IRAK4	T345	−1.11958	0.01501	−1.10131	0.02301	−1.11424	0.01401
MyD88	Y276	−1.06998	0.00799	−	−	−1.06607	0.03772
MyD88	Y257	−1.1554	0.00011	−1.12401	0.00002	−1.15724	0.00005
MyD88	S244	−1.19904	0.00007	−1.17744	0.00001	−1.22985	0.00001
NLRP3	S295	1.35545	0.00476	1.25252	0.02796	1.23998	0.04467
NFKB p100	S866	1.17578	0.0293	1.17052	0.03621	−	−
NFKB p100	S222	−1.07229	0.00348	1.2488	0.01987	1.21512	0.04191
NFKB p105	S927	1.14178	0.03856	−	−	−	−
NFKB p105	S932	−1.05462	0.00261	−1.03674	0.01158	−1.08218	0.00062
PKC $\alpha$	T638	1.14255	0.04724	−	−	−	−
PKC $\beta$	T500	1.36536	0.00684	−	−	−	−
PKC $\tau$	T538	−1.03566	0.02372	−1.08014	0.00966	−1.06587	0.00292
STAT1	Y701	−1.06177	0.00284	−1.38865	0.02834	−	−
STAT1	S727	−1.13556	0.00838	−1.28663	0.01608	−1.16671	0.00004
TBK1	S504	−1.03284	0.02015	−	−	−1.04841	0.01548
TICAM2	S16	−1.11545	0.00027	−	−	−1.05415	0.02642
TRAF2	S11	−1.05393	0.03354	−	−	−	−
TRAF3	S349	1.10998	0.03985	1.14787	0.02755	−	−
TIRAP	Y187	−1.04609	0.03097	−	−	−	−
TIRAP	Y106	−1.09487	0.00207	−1.07422	0.0052	−1.14581	0.00005
TANK	T213	−1.03559	0.01584	−	−	−1.03253	0.03618
AP-1	S63	−1.05936	0.00098	−	−	−1.08791	0.00002
AP-1	S73	−1.07448	0.01134	−	−	−	−
TRAF6	Y291	−1.11478	0	−1.19377	0.00023	−1.09779	0.00035
TRADD1	S296	−1.04853	0.03805	−1.06639	0.00308	−1.30093	0
ERK2	S67	1.11472	0.01577	1.11472	0.01577	−	−
p38	T559	1.13899	0.04897	1.13899	0.04897	−	−
p38	S352	1.18836	0.04475	1.18836	0.04475	−	−
JNK1	S400	−1.03993	0.00255	−1.03993	0.00255	−1.09831	0.00022
JNK1	T290	−1.03576	0.03682	−1.03576	0.03682	−1.0729	0.00221
NF- $\kappa$ B p65	S468	−1.22122	0.01709	−1.22122	0.01709	−	−

(Continued)

**Table 2.** Continued.

<sup>1</sup> Phosphoprotein	<sup>2</sup> Kinase target	SBDE		LPS		PGN	
		<sup>3</sup> Fold change	<sup>4</sup> P value	<sup>3</sup> Fold change	<sup>4</sup> P value	<sup>3</sup> Fold change	<sup>4</sup> P value
PI3K $\alpha$	Y528	−1.05861	0.03746	−1.05861	0.03746	−1.11927	0.00021
PI3K $\alpha$	Y556	1.16788	0.0492	1.16788	0.0492	—	—
PI3K $\beta$	Y464	1.11623	0.04944	1.11623	0.04944	—	—
NLRP1	S823	−1.26423	0.01947	−1.26423	0.01947	—	—

<sup>1</sup> Gene name for substrate protein with target peptide for phosphorylation on the array.

<sup>2</sup> Position and amino acid symbol on substrate protein.

<sup>3</sup> Fold changes for SBDE-, LPS- and PGN- treated samples were calculated by comparing the background corrected and normalized signal values to the media alone treated control samples.

<sup>4</sup> P values, as reported by Genespring software for normalized phosphorylation signals.

Differentially phosphorylated proteins that are non-significant among treatments are denoted as “—”.

SBDE: Swine Barn Dust Extracts.

**Table 3.** Differentially phosphorylated substrate peptides in SBDE-, LPS- and PGN-treated THP-1 monocyte derived macrophage cell line.

<sup>1</sup> Phosphoprotein	<sup>2</sup> Kinase target	SBDE		LPS		PGN	
		<sup>3</sup> Fold change	<sup>4</sup> P value	<sup>3</sup> Fold change	<sup>4</sup> P value	<sup>3</sup> Fold change	<sup>4</sup> P value
IFNAR2	Y512	1.00973	0.00103	1.03142	0.00182	—	—
IRF3	S386	1.09747	0	1.04321	0.00001	—	—
IRF3	S396	1.04441	0.0428	1.02134	0.04936	—	—
IRF5	S446	1.0902	0	1.02318	0.00115	—	—
IRF5	S435	1.08036	0	—	—	1.12197	0.00022
IRF7	S479	1.06657	0	—	—	1.14014	0.00016
MDA5	S88	−1.11103	0.01692	−1.02585	0.00202	—	—
IFITM1	T73	1.07195	0	—	—	1.13154	0.0005
ILIRAP	S557	1.05887	0	1.0286	0.00011	—	—
ILIRAP	S566	1.04731	0	1.01262	0.04222	1.11802	0.00018
ILIR	T210	−1.19101	0.02987	—	—	1.05025	0.00396
IRAK1	T66	1.03684	0.00013	−1.02129	0.00026	1.07143	0.02993
IRAK4	T342	1.03836	0.03556	1.01493	0.03076	—	—
MAVS	S233	−1.03764	0.00019	−1.09309	0	—	—
MAVS	T234	−1.04758	0	−1.11815	0	—	—
p38 $\beta$	T180	1.0296	0.00737	−1.03337	0.00003	—	—
p38 $\alpha$	Y182	1.05749	0.00016	−1.03111	0.00045	—	—
JNK1/3	T183	1.02942	0.0128	−1.04121	0.00034	1.05693	0.04682
JNK1/3	Y185	−1.09041	0	−1.12086	0	−1.09439	0.02944
JNK2	T183	−1.04978	0.00534	−1.08517	0	—	—
JNK2	Y185	−1.0631	0	−1.15306	0	—	—
ERK2	S67	1.08683	0	—	—	1.08542	0.00607
p38 $\alpha$	T559	1.05666	0	1.02388	0.02361	1.10525	0.00259
p38 $\alpha$	S352	1.05342	0.00015	1.04348	0.00006	—	—
ERK5	T187	1.05936	0.0129	—	—	—	—
NLRP3	S436	1.05217	0.00172	1.03051	0.0024	—	—
NEMO	S376	1.07917	0	1.01805	0.0059	—	—
NFKBIB	S19	1.05354	0.00001	—	—	1.1104	0.00026
NFKBIB	S313	1.04347	0.0001	—	—	—	—
NFKBIB	S315	1.0366	0.01302	—	—	1.01494	0.01311

(Continued)

Table 3. Continued.

<sup>1</sup> Phosphoprotein	<sup>2</sup> Kinase target	SBDE		LPS		PGN	
		<sup>3</sup> Fold change	<sup>4</sup> P value	<sup>3</sup> Fold change	<sup>4</sup> P value	<sup>3</sup> Fold change	<sup>4</sup> P value
NOS	T495	1.08529	0	1.05821	0	—	—
NLRC4	T736	1.05993	0	—	—	1.10799	0.0005
NLRX1	T428	1.08208	0.00001	1.04228	0.00003	—	—
NFKB p100	S222	1.04883	0.00017	—	—	1.07609	0.03037
NFKB p105	S932	1.02776	0.00494	—1.04799	0.00012	1.07591	0.00621
NFKB p100	S222	1.04883	0.00017	—	—	1.14081	0.00029
NFKB p105	S932	1.02776	0.00494	—1.04799	0.00012	1.07591	0.00621
PI3K $\alpha$	Y556	1.07729	0	1.03857	0.00002	—	—
PI3K $\beta$	Y464	1.03084	0.00001	1.06648	0.01333	—	—
PI3K $\beta$	Y655	—1.0375	0.00183	—	—	—	—
PI3K $\gamma$	Y199	—1.08616	0.04758	—	—	—	—
RIG-I	S8	1.05243	0	—	—	1.08686	0.00518
RIG-I	T170	1.05206	0.00034	1.0454	0.00023	—	—
RIG-I	T770	—1.13766	0.00045	—1.06072	0	—	—
RIG-I	Y518	1.06359	0	1.02215	0.01133	1.13395	0.00006
PKC $\alpha$	T638	1.04384	0.00237	1.06028	0	—	—
PKC $\alpha$	S657	1.01379	0.02943	—1.03239	0.00056	1.0744	0.0069
PKC $\alpha$	S226	—1.09638	0.0272	—	—	—	—
PKC $\beta$	S661	—1.04009	0.0066	—1.03851	0.00451	—	—
PKC $\beta$	T500	—1.12464	0.0016	—1.04443	0.00016	—	—
PKC $\delta$	Y64	1.06633	0	1.03257	0.00001	1.08737	0.01538
PKC $\delta$	T507	—1.15968	0.02165	—1.01995	0.01586	—	—
PKC $\tau$	S676	1.08073	0	—	—	1.08631	0.01125
PKC $\tau$	Y90	—1.13879	0.03694	—1.05094	0.00001	—	—
PKC $\zeta$	T560	1.03979	0.00006	—	—	1.1124	0.0005
PKC $\zeta$	T410	1.02156	0.00036	—	—	1.06595	0.0273
STAT1	Y701	1.01877	0.02734	—1.03587	0.0001	1.09672	0.00224
TBKBPI	S372	1.05527	0	—	—	1.09265	0.00239
TBKBPI	S504	1.0461	0	—1.01263	0.04508	1.07613	0.00338
TICAM1	S199	1.0387	0.00618	—1.0178	0.04046	—	—
TICAM2	S16	1.06706	0	—	—	—	—
TRAF1	Y310	1.05909	0	1.04101	0.00002	1.17223	0
TRAF2	S11	1.02979	0.04035	—	—	1.07316	0.03934
TRAF6	S507	1.06696	0	1.02068	0.02471	1.11318	0.00055
TIRAP	Y187	1.07316	0	—	—	1.08795	0.00601
TIRAP	Y86	—1.18712	0.00001	—1.14293	0	—1.39469	0.02829
TLR2	Y653	—1.18313	0.03174	1.01921	0.00929	1.06423	0.02671
TLR4	Y674	—1.06232	0.00268	—1.02676	0.00039	—	—
TLR4	Y680	—1.20141	0.00814	—1.02728	0.01298	—	—
TLR5	Y798	1.10796	0	1.06862	0	1.20677	0
TLR6	Y648	—1.19214	0.0025	—1.04418	0.00044	—	—
TLR7	S371	1.08492	0	—1.04418	0.00044	1.1032	0.00147
TLR8	Y886	—1.0172	0.01984	—1.0398	0.00008	—	—
TLR9	Y345	—1.0726	0.00003	—1.03303	0.00109	—	—
TANK	T213	1.07172	0	—	—	1.09426	0.00045
TANK	S225	—1.09547	0.01904	—	—	—	—
AP-1	S63	1.06502	0	1.03663	0.00049	1.1455	0.00004

(Continued)

**Table 3.** Continued.

<sup>1</sup> Phosphoprotein	<sup>2</sup> Kinase target	SBDE		LPS		PGN	
		<sup>3</sup> Fold change	<sup>4</sup> P value	<sup>3</sup> Fold change	<sup>4</sup> P value	<sup>3</sup> Fold change	<sup>4</sup> P value
NF- $\kappa$ B p65	S276	1.06812	0	1.02129	0.00245	1.07179	0.04601
TRADD	S215	1.07367	0	1.02951	0.00993	1.10106	0.00391
TRADD	S296	-1.18043	0	-1.12304	0	-1.08267	0.0023

<sup>1</sup>Gene name for substrate protein with target peptide for phosphorylation on the array.

<sup>2</sup>Position and amino acid symbol on substrate protein.

<sup>3</sup>Fold changes for SBDE-, LPS- and PGN-treated samples were calculated by comparing the background corrected and normalized signal values to the media alone treated control samples.

<sup>4</sup>P values, as reported by Genespring software for normalized phosphorylation signals.

Differentially phosphorylated proteins that are non-significant among treatments are denoted as “-”.

SBDE: Swine Barn Dust Extracts.

NF- $\kappa$ B and AP-1 family of transcription factors (Table 2). MyD88 serves as an adaptor for TLR2, TLR4, TLR5, TLR7/8/9 whereas TLR4 can also signal via TRIF/TIRAP to activate downstream kinase complex TBK1/IKK $\epsilon$ , responsible for activation of IFN regulatory factors (IRF3 and 7) leading to Type I IFN production. TLR4-TICAM-TRAF3-dependent IRF3/7 activation pathway also appears to be active, resulting in Type I IFN release and subsequent activation of IFN- $\alpha$  receptor and STAT1. Type I IFNs act in auto or paracrine manner to induce transcriptional activation of IFN-stimulated genes, among them include IFN-induced transmembrane protein 1 (IFITM1) which was found to be differentially phosphorylated (Table 2).

Based on the observed activation of IFN induction and downstream Type I IFN signaling pathways, we evaluated mRNA expression levels of Type I IFNs (IFN- $\beta$ , - $\alpha$ ) and one of the downstream effectors of IFN signaling (IFIT1). Interestingly, we found a significant induction of IFN- $\alpha$  but not IFN- $\beta$  (Figure 1). However, no downstream IFN-induced signaling was observed as seen with a lack of induction of IFIT1 (IFIT1 threshold cycles remained > 35 among all the study treatments in both BEAS-2B and THP-1 cell lines). As expected, a lack of Type I IFNs and IFN signaling was also evident in controls, LPS- and PGN-treated cells, whose responses are primarily pro-inflammatory with no or little amounts of Type I IFNs.

TLR2, upon stimulation with heat-killed *S. aureus*, is known to activate NF- $\kappa$ B in a Rac1-PI3K-dependent manner in THP-1 cells.<sup>34</sup> This pathway appears to be active in the SBDE-treated BEAS-2B cell line (Table 2). Finally, both TLR2 and TLR4 pathways appear to be activated in response to SBDE in the BEAS-2B cell line. Additionally, various TLR ligands are known to stimulate downstream activation of MAPKs such as ERK1/2, JNK and p38, with all three of them found to be differentially phosphorylated in SBDE-treated cells (Table 2).<sup>35</sup> LPS-treated BEAS-2B cells have shown proliferative response via thymidine [ $H^{3+}$ ]

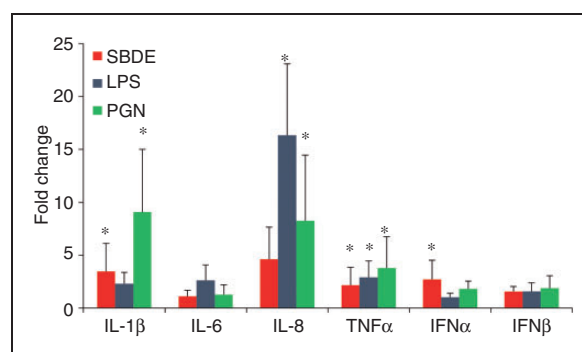


**Figure 1.** Relative cytokine gene expression in BEAS-2B cells treated with SBDE (red bars), LPS (blue bars) and PGN (green bars). Error bars indicate standard deviation and asterisk denotes statistical significance ( $P < 0.05$ ). Y-Axis indicates mRNA fold change compared with media treated control. Target gene expression was normalized to endogenous reference GAPDH. SBDE: Swine Barn Dust Extracts.

incorporation in a p38, JNK and PI3K dependent manner whereas this effect was ERK1/2-independent.<sup>36</sup>

There was a significant enrichment of pathways related to cancer, among which protein kinase signaling mediated by PKC and PKA are evident. PKC and PKA signaling occur downstream of GPCR activation and play agonistic and antagonistic roles, respectively, in promoting IL-6 induction during SBDE exposure.<sup>13</sup> Finally, studies have shown that TLR-mediated Tpl2 activation activates ERK1/2 through MEK3/6 phosphorylation and this event regulates nucleocytoplasmic shuttling of TNF- $\alpha$  mRNA.<sup>37</sup> Both Tpl-ERK1/2 and TNF- $\alpha$  signaling were significantly enriched in our study (Table 3). Congruent with TNF- $\alpha$  signaling and PKC activation, TNF- $\alpha$  mRNA was > 2-fold up-regulated. IL-6 mRNA levels however, remained at basal levels (Figure 1). TNF- $\alpha$  mRNA levels in SBDE-treated cells were comparable with LPS- and PGN-treated cells.

As epithelial cells are the first cells that respond to organic dust, chemokine signaling is not unusual.



Chemokines produced by these cells function in autocrine or paracrine manner to recruit other innate cells such as neutrophils (CXCL8) and monocytes (MCP1). By virtue of this, we decided to quantify key chemokines involved in neutrophil influx and airway pathology, IL-8 (CXCL8).<sup>1,18,22,23</sup> Although not significant, we observed a 4.6-fold induction of IL-8 mRNA in SBDE-treated cells. A greater level of induction was seen in LPS-treated cells followed by PGN controls (Figure 1). The differentially phosphorylated receptor on the array was CXCR3. This is consistent with the constitutive expression of CXCR3 on HBEC.<sup>38</sup> HBEC also produce CXCR3 ligands in response to pro-inflammatory cytokines such as TNF- $\alpha$ . In line with this, TNF- $\alpha$  receptor signaling was found to be activated with subsequent downstream activation of the NF- $\kappa$ B/AP-1 family of transcription factors (Table 2). CXCR3 is a GPCR which upon ligand activation appears to stimulate cell proliferation under normal conditions. However, under pro-inflammatory milieu, it may inhibit epithelial cell proliferation leading to airway mucosal denudation and damage which appear to be the predominant mechanism in play, based on our results.<sup>38</sup> CXCR3 activation leads to downstream activation of PI3K and MAPK (ERK1/2 and p38 arms), both of which were found to be differentially phosphorylated (Table 2).<sup>38</sup>

Lastly, we also found a significant enrichment of pathways related to inflammasome activation (Tables 1 and 2). NLRs, NLRP3 and NLRP1 were found differentially phosphorylated on our array. NLRP3 is activated via wide array of ligands including microbial (pore-forming toxins) host derived (ATP, urate, mitochondrial DNA (mtDNA), K<sup>+</sup>) and sterile substances (silica, asbestos, alum). Furthermore, brief LPS stimulation appears to activate NLRP3 independent of its transcriptional induction. This mode of activation is dependent on mitochondrial ROS and is further potentiated by ligand ATP.<sup>39,40</sup> NLRP3 activation leads to ASC-mediated caspase 1 activation which processes pro-forms of IL-1 $\beta$  and IL-18 into mature secretory forms. In line with this, downstream activation of IL-1 R was seen. NLRP3 inflammasome activation and IL-1 family cytokine production are regulated at transcriptional and post transcriptional levels. A two signal model for NLRP3 activation indicates initial priming or the first signal being microbial or cytokine molecules that induce NLRP3 and pro-IL-1 $\beta$  mRNA via NF- $\kappa$ B activation followed by a second signal or NLRP3 activation triggered by NLRP3 ligands ATP, pore-forming toxins, viral RNA, or particulate matter.<sup>41,42</sup> We investigated the priming signal by quantifying IL-1 $\beta$  mRNA levels and found a significant induction in SBDE-treated cells. In addition, a non-significant up-regulation and a significant up-regulation of IL-1 $\beta$  mRNA was

found in LPS- and PGN-treated cells, respectively (Figure 1).

To identify protein interaction networks among the differentially phosphorylated proteins in SBDE-treated BEAS-2B cells and to connect them to the molecular networks deposited within the Ingenuity Knowledge Base, which contains biological interactions and functional annotations derived from literature or verified experimental models, we used IPA. IPA identified the top enriched molecular network to contain proteins with functions in cell signaling, inflammatory response, and antimicrobial response (score, 29; number of focus proteins in network, 17). Several protein hubs displayed high connectivity among others in the network (>8 direct or indirect connections), which included hubs involved in signal transduction by TLR (MyD88, IRAK4, IRAK1, TIRAP), IFN transcription (IRF-3, -5, -7), cytokine-mediated signaling (IL-1 R, IFNGR1, IFNAR) and chemokine signaling (CXCR3) (Figure 2a). In the second (score, 25; focus molecules, 15) and third (score, 25; focus molecules, 15) networks, proteins enriched in our kinome data set connected to major regulators of inflammation, such as inflammasome, NF- $\kappa$ B, STAT3, TNF- $\alpha$  and caspases (Figure 2b, 2c).

#### *LPS-induced kinome signaling in BEAS-2B cell line*

In BEAS-2B cells treated with LPS there was a stark enrichment of canonical TLR4 pathway. In addition, an activation of TLR2 signaling was also observed (Table 2). This could be due to cross talk among TLR signaling pathways or possible contamination of the LPS with other TLR ligands. In any case, the downstream consequence of signal integration was activation of NF- $\kappa$ B/AP-1 and IRF3 transcription factors. Lending further support, there was an activation of IFN- $\alpha$ / $\beta$  receptor and downstream STAT1 indicating interferon responsiveness. Other pathways enriched included NF- $\kappa$ B (IL-1 R) and TNF- $\alpha$  receptor signaling, while the latter is interdependent on the former activation. Unsurprisingly, cancer pathways, similar to our observation in SBDE-treated cells, were found to be enriched indicating putative role played by LPS in stimulating cell proliferation.

#### *PGN-induced kinome signaling in BEAS-2B cell line*

In BEAS-2B cells treated with PGN, similar to the cross-talk patterns observed in the LPS-treated cells, there is an activation of TLR2 and TLR4 signaling. Consistent with the former, an enrichment of TNF- $\alpha$  signaling and chemokine signaling was observed (Table 2). Finally, cancer pathways commonly observed among the other two treatments (SBDE and LPS) were seen.

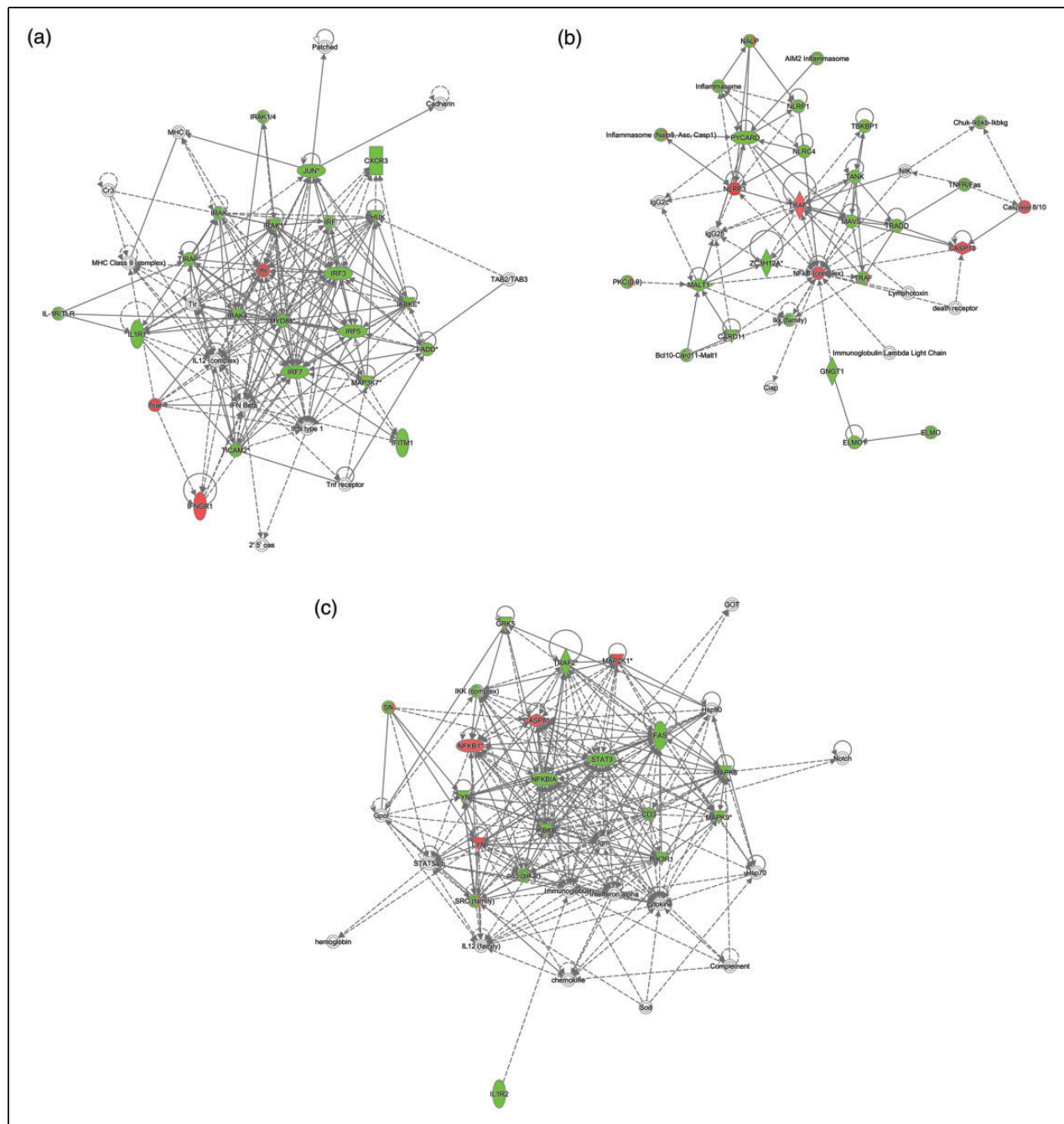


**Figure 2.** The top three enriched networks of interacting proteins in SBDE-treated BEAS2B cells, as determined by IPA. These networks were defined as: (a) cell signaling, inflammatory response, antimicrobial response (score, 29; 17 differentially phosphorylated proteins); (b) Cell signaling, cellular function and maintenance, cell death and survival (score, 25; 15 differentially phosphorylated proteins); (c) Cell death and survival, organismal injury and abnormalities, gastrointestinal disease (score, 25; 15 differentially phosphorylated proteins). Proteins represented in green (decreased) and red (increased) were differentially phosphorylated on the kinome array relative to control untreated cells. Proteins shown in white were not present in our data set but were added by IPA due to their connection to the enriched proteins. Scores were calculated from hypergeometric distribution and right-tailed Fisher's exact test. SBDE: Swine Barn Dust Extracts; IPA: Ingenuity Pathway Analysis.

### SBDE-induced kinome signaling in THP-1 cell line

In THP-1 cells treated with SBDE, interesting clusters that yield valuable information were observed. Although TLR signaling was one of the enriched

pathways, we found novel signaling pathways that were not observed in BEAS-2B cells treated with SBDE. These include TLR5, TLR7/8 and TLR9 (Table 3). As a readout for TLR-mediated downstream activation of NF- $\kappa$ B, we investigated mRNA

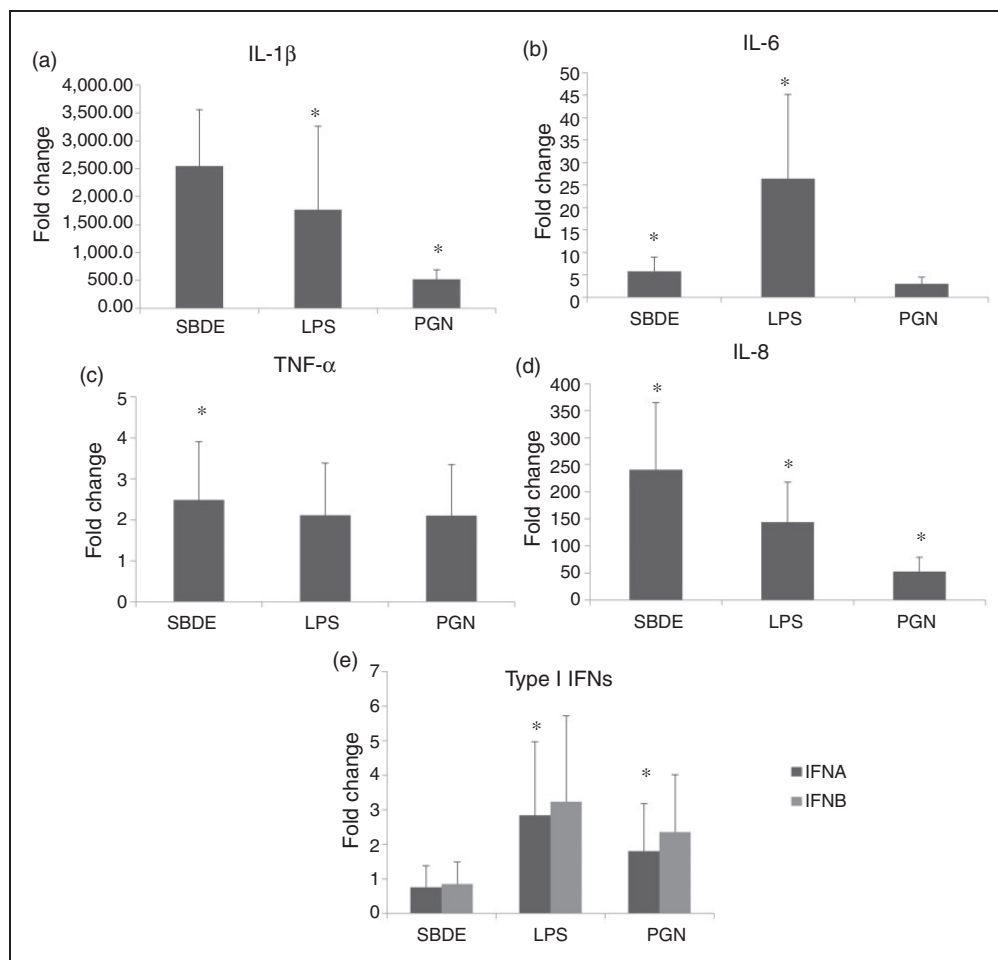


**Figure 3.** Relative cytokine gene expression in THP-1 cells treated with SBDE, LPS and PGN. Panels a, b, c, d and e depict IL-1 $\beta$ , IL-6, TNF- $\alpha$ , IL-8 and Type I IFNs ( $\alpha$ ,  $\beta$ ), respectively. Error bars indicate standard deviation and asterisk denotes statistical significance ( $P < 0.05$ ). Y-axis indicates mRNA fold change compared with media treated controls. Target gene expression was normalized to endogenous reference GAPDH.

SBDE: Swine Barn Dust Extracts.

expression levels of pro-inflammatory cytokines (IL-1 $\beta$ , IL-6 and TNF- $\alpha$ ) and chemokines (IL-8). A greater level of IL-1 $\beta$  and IL-8 was observed in SBDE-treated cells compared with LPS- and PGN-treated controls (Figure 3a, b and e). Furthermore, significant induction of both IL-6 and TNF- $\alpha$  was observed in SBDE-treated cells (Figure 3c and d). In addition, endosomal TLRs, TLR7/8 and TLR9 that recognize ssRNA and unmethylated bacterial CpG DNA sequences, respectively, were found to be differentially phosphorylated. Based on the enrichment of aforementioned pathways, the dust-associated dander may presumably encompass RNA and CpG DNA originating from viruses and bacteria, respectively.

A significant enrichment of pathways related to viral infections (IAV and HCV) was found (Table 4). Among these, one common trend observed was RIG1/MDA5-IPS1-TBK1/IKK $\epsilon$ -IRF3-IFN- $\beta$ / $\alpha$  axis. RIG1 and MDA5 are cytoplasmic PRRs that recognize and respond to short and long dsRNAs,

respectively, and signal via IPS-1/MAVS to produce Type I IFNs. Since RIG1/MDA5 play an important role in the control of aforementioned viruses, these pathways appear to be enriched, although the actual presence of these viruses in SBDE is irrelevant. In fact, a recent study indicates airborne influenza A virion (80–120 nm) bound to organic dust or other particulate matter in the swine barn.<sup>43</sup> To determine the relevance of Type I IFN production, we examined the mRNA expression levels of Type I IFNs (IFN- $\beta$ ,  $\alpha$ ) and downstream IFIT1. No significant induction of either was observed similar to responses seen in BEAS-2B cells (Figure 3E). THP-1 and BEAS-2B cells differed significantly in the cytokine mRNA profiles. Expression levels of IL-1 $\beta$ , IL-6 and IL-8 were several folds greater in magnitude in THP-1 cells compared with BEAS-2B cells.

Using IPA, we identified protein interaction networks among the differentially phosphorylated proteins in SBDE-treated THP-1 cells and connected the

**Table 4.** DAVID GO-term enrichment of innate immune pathways in THP-1 cell line treatments.

SBDE	LPS	PGN
hsa04620: TLR signaling	hsa04620: TLR signaling	hsa04620: TLR signaling
hsa04668: TNF- $\alpha$ signaling	hsa04668: TNF- $\alpha$ signaling	hsa05142: Chagas disease
hsa05161: Hepatitis B	hsa05142: Chagas disease	hsa05145: Toxoplasmosis
hsa05164: Influenza A	hsa05145: Toxoplasmosis	hsa04668: TNF- $\alpha$ signaling
hsa05160: Hepatitis C	hsa05169: Epstein-Barr virus infection	hsa04210: Apoptosis

DAVID: Database for Annotation, Visualization and Integrated Discovery.

proteins to molecular networks contained within the Ingenuity Knowledge Base. Upon molecular network analysis, IPA identified the top enriched molecular network to contain proteins involved in cell signaling, gene expression, cell death, survival (score, 294; focus proteins in network, 16). Protein hubs that displayed high connectivity in the network (>8 direct or indirect connections), include those involved in signal transduction by TNFR (TRAF, TRADD, TAB1), in line with the transcriptional induction of TNF- $\alpha$  (Figure 3d, Figure 4a). In the second (score, 24; focus molecules, 16) and third (score, 24; focus molecules, 16) networks, proteins enriched in our kinome data set connected to cellular reorganization and cell death, respectively (Figure 4b and c), implicating macrophage-mediated tissue reorganization due to SBDE-exposure-mediated airway pathology.

#### LPS-induced kinome signaling in THP-1 cell line

In THP-1 cells treated with LPS, canonical TLR4 signaling was seen. Additionally, due to cross talk among TLR receptors or possible contamination of the LPS with other TLR ligands, TLR2 and TLR5 activation was also observed (Table 3). TLR signaling leads to downstream activation of NF- $\kappa$ B and TNF- $\alpha$  production. In line with this, TNF- $\alpha$  receptor and the downstream targets were found to be differentially phosphorylated. Other enriched pathways include pathways related to Epstein Barr virus infection (EBV), and parasitic infections (Chagas disease caused by *Trypanosoma cruzi* and Toxoplasmosis caused by *Toxoplasma gondii*) due a significant overlap of these pathways with TLR and downstream NF- $\kappa$ B activation leading to their overrepresentation (Table 4).

#### PGN-induced kinome signaling in THP-1 cell line

In THP-1 cells treated with PGN, TLR2 signaling was seen (Table 3). Additionally, due to cross talk among TLR receptors, TLR5 activation was also observed. Other enriched pathways include pathways related to parasitic infections (Chagas disease and Toxoplasmosis) and TNF- $\alpha$  receptor signaling (Table 4).

## Discussion

In this manuscript, we report on various cell-signaling pathways activated upon treatment of human airway epithelial or macrophage cells with SBDE or LPS or PGN. Our work highlights the complexity of SBDE constituents and SBDE-induced host response through activation of multiple PRRs-related pathways. Upon comparison of differential phosphorylation profiles of SBDE, LPS or PGN treatment, common trends observed include TLR2 and TLR4 activation, NF- $\kappa$ B signaling, TNF- $\alpha$  receptor signaling and chemokine signaling. These trends indicate significant amounts of TLR2 and 4 ligands in SBDE. Furthermore, although the contributory role played by endotoxin is thought to be minor, apart from TLR4 activation, LPS also contributes to the priming and activation of NLRP3 inflammasome. In addition, muramyl dipeptide, a constituent of Gram-positive cell walls, is known to activate NLRP1 in the presence of NOD2, leading to IL-1 $\beta$  secretion. The presence of other NLR ligands in the SBDE extracts is unknown. Finally, inflammasomes play an important role in the pathogenesis of many respiratory diseases such as ARDS, COPD, fibrotic lung disease and lung cancer. Based on the pathway responses seen in our study, it appears that chronic activation of TLRs and inflammasomes by SBDE appears to provide primary and secondary signals necessary for pro-inflammatory IL-1 $\beta$  production. This is corroborated by the observed induction of IL-1 $\beta$  mRNA in both BEAS-2B and THP-1 cell lines. On the other hand, TLR-mediated activation of NF- $\kappa$ B leads to IL-6, IL-8 (CXCL8) and TNF- $\alpha$  production. IL-8 is a chemotactic cytokine responsible for neutrophil influx and subsequent immune-related pathology seen in airways upon chronic exposure to barn dust.

In THP-1 cells, additional TLR and RLR pathways were enriched, indicating the presence of respective ligands. These include TLR5, TLR7/8, TLR9, RIG-I, MDA5 and MAVS. Besides TLR2 and TLR4, TLR5 is activated by flagellin proteins found in Gram-negative bacteria. In fact, highly purified recombinant flagellin (rFLA) was found to sensitize mice to allergic inflammation when administered with OVA.<sup>44</sup> In the same study, TLR5 was shown to be required for



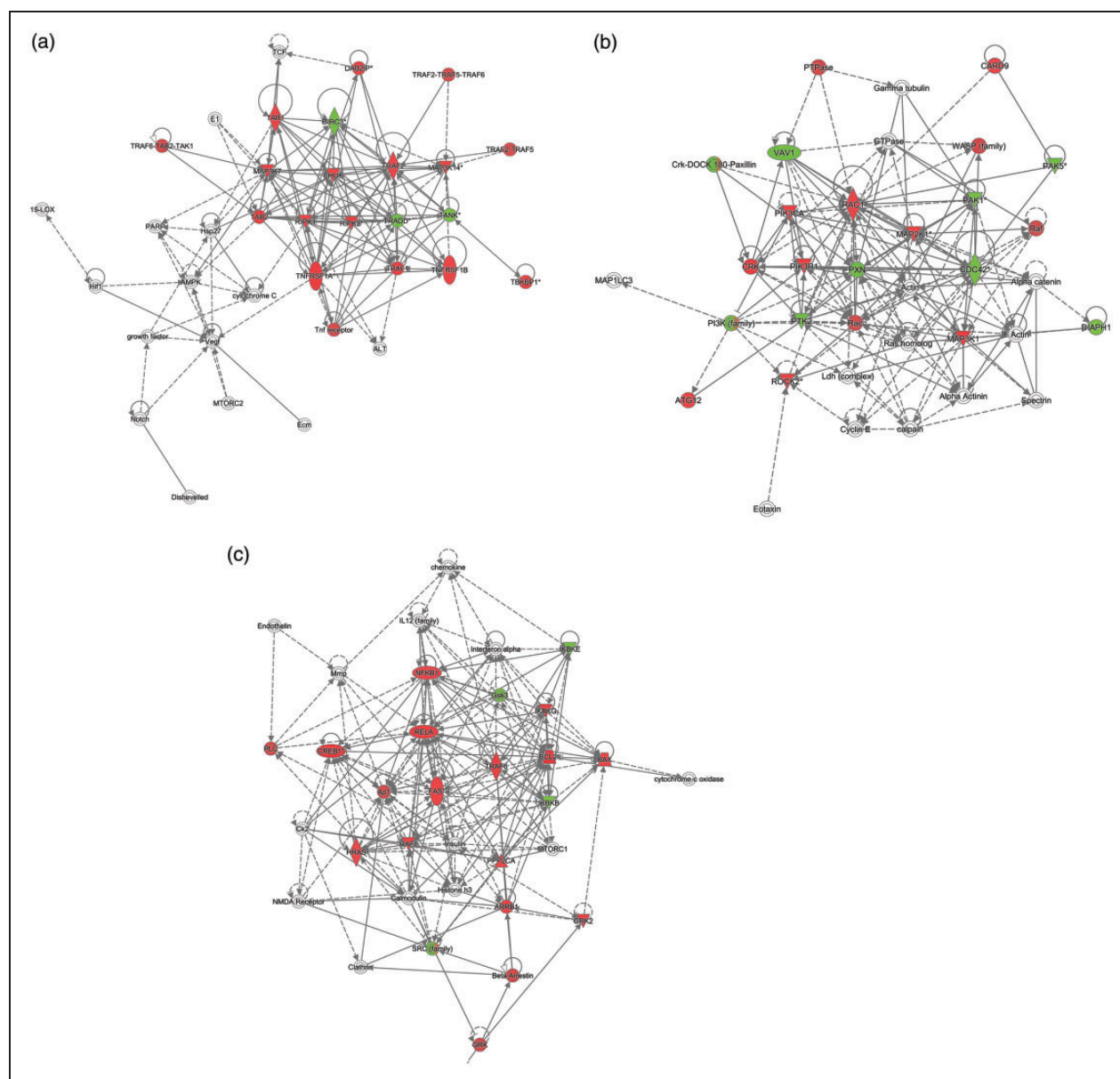


**Figure 4.** The top three enriched networks of interacting proteins in SBDE-treated THP-1 cells, as determined by IPA. These networks were defined as: (a) cell signaling, gene expression, cell death, survival (score, 24; 16 differentially phosphorylated proteins); (b) Cellular assembly, organization, cellular function and maintenance, tissue development (score, 24; 16 differentially phosphorylated proteins); (c) Cell death and survival, gastrointestinal disease, hepatic system disease (score, 24; 16 differentially phosphorylated proteins). Proteins represented in green (decreased) and red (increased) were differentially phosphorylated on the kinome array relative to control untreated cells. Proteins shown in white were not present in our data set but were added by IPA due to their connection to the enriched proteins. Scores were calculated from hypergeometric distribution and right-tailed Fisher's exact test. SBDE: Swine Barn Dust Extracts; IPA: Ingenuity Pathway Analysis.

priming strong allergic responses to natural indoor allergens present in house dust extracts (HDEs). The role of TLR5 in barn dust-induced airway inflammation was not investigated. However, the presence of flagellin proteins or fragments in the barn dust cannot be excluded and necessitates detailed investigation. Henceforth, the putative role played by their respective ligands and downstream pathway activation during airway inflammation begs further investigation. This

result is an important future avenue of research on the effects of swine barn dust and may lead to additional targets of intervention by reducing TLR5 responses in exposed individuals.

In our study, however, we observed a lack of RIG-I- and MDA5-mediated Type I IFN induction or downstream IFN signaling in THP-1 cells. On the other hand, in BEAS-2B cells a significant induction of Type I IFNs with a lack of downstream IFN signaling



was observed. Nevertheless, a lack of downstream interferon signaling indicated by an absence of IFIT1 induction suggests no significant role played by Type I IFNs in SBDE-mediated inflammation. Furthermore, our efforts to amplify viral (IAV) RNA (RIG-I ligand) in SBDE inoculum remained futile. Henceforth, airway pathology seen upon chronic exposure to barn dust is predominantly pro-inflammatory cytokine mediated, including IL-8-mediated neutrophil influx. Based on the responses seen in BEAS-2B and THP-1 cells, both bronchial epithelial cells and resident alveolar macrophages appear to play a critical role in IL-8 production and neutrophil influx. We observed a significantly stronger immune activation both at the gene expression and kinome levels in THP-1 cells compared with BEAS-2B cells. This may be due to the greater activation potential of macrophage compared with epithelial cells, it also may indicate that while activated macrophages are highly inflammatory, epithelial cells require a more balanced and tolerant response to the constant exposure to immune ligands.

To dissect the specific pathways enriched by the SBDE other than those mediated by TLR4 and TLR2, we performed pathway enrichment analyses on the basis of mutual exclusion. Significant phosphorylation events that are either up- or down-regulated among all treatments were excluded whereas those events that exhibit temporal changes in at least one of the three treatments were retained for analyses. In this scenario, a higher number of events was detected in SBDE-treated THP-1 cells when compared with SBDE-treated BEAS-2B cells (453 vs 31). Enriched pathways upon exclusion in BEAS-2B cell line include cancer pathways, chemokine, VEGF, NF- $\kappa$ B,  $\text{Ca}^{2+}$ , TNF- $\alpha$  and leucocyte trans-endothelial migration signaling pathways (data not shown). These pathways describe potent activation of downstream NF- $\kappa$ B and production of chemokines leading to further recruitment of other leukocytes such as neutrophils. In THP-1 cells, enriched pathways upon exclusion include cancer pathways, chemokine, TLR, RLR, NF- $\kappa$ B, TNFR apoptosis related, TNF- $\alpha$  and leucocyte trans-endothelial migration signaling pathways (data not shown). Additional activation of TLR5, TLR7/8, TLR9, RIG-I and MDA5 seen in THP-1 cells, is reiterated upon exclusion-based analyses.

Collectively, our kinome array data indicates that SBDE is a potent stimulator of pro-inflammatory cytokine production with greater levels of IL-8 secreted by BEAS-2B and THP-1 cells. In agreement with this, a recent study reported greater levels of IL-8 secretion by lung epithelial (BEAS-2B and A549) and THP-1 monocyte cell lines treated with poultry dust extract.<sup>9</sup> Furthermore, IL-8 induction was reported to be associated with activation of PKC and MAPK and binding

of AP1 and NF- $\kappa$ B to IL-8 promoter, all of which were identified to be differentially phosphorylated on our arrays. Targeting the IL-8 response either by inhibiting up-stream pathway activation or inhibiting the IL-18 cytokine by anti-IL-8 therapies may prove beneficial in reducing the effects of swine barn dust exposure. Our kinome and gene expression analyses data in BEAS-2B and THP-1 were quite similar to the effects in dust-exposed primary normal human bronchial cells and human peripheral blood monocytes, respectively, attesting that pro-inflammatory effects of SBDE are independent of the nature of cell type employed.<sup>22</sup> The multiple immune ligands found in SBDE and the activation of multiple receptors makes the immune response to SBDE complex. In this study we have described the multiple and overlapping signal transduction pathways, with the goal of better characterizing the immune response to SBDE. Swine confinement unit workers exposed to persistent barn air are at occupational risk of developing a range of respiratory illnesses and there is a critical need to understand the mechanisms behind those illnesses.

### Acknowledgements

The authors thank Dr Locke A Karriker (VDPAM, Iowa State University) for help with the collection of swine barn dust samples.

### Declaration of conflicting interests

The author(s) declared no potential conflicts of interest with respect to the research, authorship, and/or publication of this article.

### Funding

The author(s) disclosed receipt of the following financial support for the research, authorship, and/or publication of this article: funding from Iowa State University to C Charavaryamath and from the University of Delaware to R J Arsenault.

### ORCID iD

Sabari Nath Neerukonda  <http://orcid.org/0000-0002-1049-1929>

Ryan J Arsenault  <http://orcid.org/0000-0002-4534-278X>

### References

1. Eduard W, Pearce N and Douwes J. Chronic bronchitis, COPD, and lung function in farmers: the role of biological agents. *Chest* 2009; 136(3): 716–725.
2. Charavaryamath C, Juneau V, Suri SS, et al. Role of Toll-like receptor 4 in lung inflammation following exposure to swine barn air. *Exp Lung Res* 2008; 34(1): 19–35.
3. Senthilselvan A, Zhang Y, Dosman JA, et al. Positive human health effects of dust suppression with canola oil in swine barns. *Am J Respir Crit Care Med* 1997; 156(2): 410–417.
4. Pedersen S, Nonnenmann M, Rautiainen R, et al. Dust in pig buildings. *J Agric Saf Health* 2000; 6(4): 261–274.

5. Nehme B, Gilbert Y, Letourneau V, et al. Culture-independent characterization of archaeal biodiversity in swine confinement building bioaerosols. *Appl Environ Microbiol* 2009; 75(17): 5445–5450.
6. Nehme B, Letourneau V, Forster RJ, et al. Culture-independent approach of the bacterial bioaerosol diversity in the standard swine confinement buildings, and assessment of the seasonal effect. *Environ Microbiol* 2008; 10(3): 665–675.
7. Boissy RJ, Romberger DJ, Roughead WA, et al. Shotgun pyrosequencing metagenomic analyses of dusts from swine confinement and grain facilities. *PLoS ONE* 2014; 9(4): e95578.
8. Poole JA, Dooley GP, Saito R, et al. Muramic acid, endotoxin, 3-hydroxy fatty acids, and ergosterol content explain monocyte and epithelial cell inflammatory responses to agricultural dusts. *J Toxicol Environ Health A* 2010; 73(10): 684–700.
9. Gottipati KR, Bandari SK, Nonnenmann MW, et al. Transcriptional mechanisms and protein kinase signaling mediate organic dust induction of IL-8 expression in lung epithelial and THP-1 cells. *Am J Physiol Lung Cell Mol Physiol* 2015; 308(1): L11–L21.
10. Cormier Y, Duchaine C, Israel-Assayag E, et al. Effects of repeated swine building exposures on normal naive subjects. *Eur Respir J* 1997; 10(7): 1516–1522.
11. Essen SGV, O'Neill DP, Olenchok SA, et al. Grain dusts and grain plant components vary in their ability to recruit neutrophils. *J Toxicol Environ Health Sci* 1995; 46(4): 425–441.
12. Romberger DJ, Heires AJ, Nordgren TM, et al. beta2-Adrenergic agonists attenuate organic dust-induced lung inflammation. *Am J Physiol Lung Cell Mol Physiol* 2016; 311(1): L101–L110.
13. Romberger DJ, Heires AJ, Nordgren TM, et al. Proteases in agricultural dust induce lung inflammation through PAR-1 and PAR-2 activation. *Am J Physiol Lung Cell Mol Physiol* 2015; 309(4): L388–L399.
14. Wyatt TA, Poole JA, Nordgren TM, et al. cAMP-dependent protein kinase activation decreases cytokine release in bronchial epithelial cells. *Am J Physiol Lung Cell Mol Physiol* 2014; 307(8): L643–L651.
15. Bailey KL, Poole JA, Mathisen TL, et al. Toll-like receptor 2 is upregulated by hog confinement dust in an IL-6-dependent manner in the airway epithelium. *Am J Physiol Lung Cell Mol Physiol* 2008; 294(6): L1049–L1054.
16. Poole JA, Wyatt TA, Kielian T, et al. Toll-like receptor 2 regulates organic dust-induced airway inflammation. *Am J Respir Cell Mol Biol* 2011; 45(4): 711–719.
17. Demanche A, Bonlokke J, Beaulieu MJ, et al. Swine confinement buildings: effects of airborne particles and settled dust on airway smooth muscles. *Ann Agric Environ Med* 2009; 16(2): 233–238.
18. Poole JA, Wyatt TA, Oldenburg PJ, et al. Intranasal organic dust exposure-induced airway adaptation response marked by persistent lung inflammation and pathology in mice. *Am J Physiol Lung Cell Mol Physiol* 2009; 296(6): L1085–L1095.
19. Von Scheele I, Larsson K and Palmberg L. Budesonide enhances Toll-like receptor 2 expression in activated bronchial epithelial cells. *Inhal Toxicol* 2010; 22(6): 493–499.
20. Farkas L, Stoelcker B, Jentsch N, et al. Muramyl dipeptide modulates CXCL-8 release of BEAS-2B cells via NOD2. *Scand J Immunol* 2008; 68(3): 315–322.
21. Muller L and Jaspers I. Epithelial cells, the “switchboard” of respiratory immune defense responses: effects of air pollutants. *Swiss Med Wkly* 2012; 142: w13653.
22. Romberger DJ, Bodlak V, Von Essen SG, et al. Hog barn dust extract stimulates IL-8 and IL-6 release in human bronchial epithelial cells via PKC activation. *J Appl Physiol* 2002; 93(1): 289–296.
23. Schneberger D, Gordon JR, DeVasure JM, et al. CXCR1/CXCR2 antagonist CXCL8(3-74) K11R/G31P blocks lung inflammation in swine barn dust-instilled mice. *Pulm Pharmacol Ther* 2015; 31: 55–62.
24. Poole JA, Alexis NE, Parks C, et al. Repetitive organic dust exposure in vitro impairs macrophage differentiation and function. *J Allergy Clin Immunol* 2008; 122(2): 375–82, 82 e1–e4.
25. Knetter SM, Tuggle CK, Wannemuehler MJ, et al. Organic barn dust extract exposure impairs porcine macrophage function in vitro: Implications for respiratory health. *Vet Immunol Immunopathol* 2014; 157(1–2): 20–30.
26. Reddel RR, Ke Y, Gerwin BI, et al. Transformation of Human Bronchial Epithelial Cells by Infection with SV40 or Adenovirus-12 SV40 Hybrid Virus, or Transfection via Strontium Phosphate Coprecipitation with a Plasmid Containing SV40 Early Region Genes. *Cancer Res* 1988; 48(7): 1904–1909.
27. Tsuchiya S, Yamabe M, Yamaguchi Y, Kobayashi Y, Konno T and Tada K. Establishment and characterization of a human acute monocytic leukemia cell line (THP-1). *Int J Cancer* 1980; 26(2): 171–176.
28. Gottipati KR, Bandari SK, Nonnenmann MW, et al. Transcriptional mechanisms and protein kinase signaling mediate organic dust induction of IL-8 expression in lung epithelial and THP-1 cells. *Am J Physiol Lung Cell Mol Physiol* 2015; 308(1): L11–L21.
29. Arsenault RJ, Jalal S, Babiuk LA, et al. Kinome analysis of Toll-like receptor signaling in bovine monocytes. *J Recept Signal Transduct Res* 2009; 29(6): 299–311.
30. Arsenault RJ, Li Y, Bell K, et al. Mycobacterium avium subsp. paratuberculosis inhibits gamma interferon-induced signaling in bovine monocytes: insights into the cellular mechanisms of Johne's disease. *Infect Immun* 2012; 80(9): 3039–3048.
31. Pfaffl MW, Horgan GW and Dempfle L. Relative expression software tool (REST) for group-wise comparison and statistical analysis of relative expression results in real-time PCR. *Nucleic Acids Res* 2002; 30(9): e36.
32. Neerukonda SN, Katneni UK, Golovan S, et al. Evaluation and validation of reference gene stability during Marek's disease virus (MDV) infection. *J Virol Methods* 2016; 236: 111–116.
33. Huang DW, Sherman BT, Tan Q, et al. The DAVID Gene Functional Classification Tool: a novel biological module-centric algorithm to functionally analyze large gene lists. *Genome Biol* 2007; 8(9): R183.
34. Arbibe L, Mira JP, Teusch N, et al. Toll-like receptor 2-mediated NF-kappa B activation requires a Rac1-dependent pathway. *Nat Immunol* 2000; 1(6): 533–540.
35. Kawai T and Akira S. TLR signaling. *Cell Death Differ* 2006; 13(5): 816–825.
36. Verspohl EJ and Podlogar J. LPS-Induced Proliferation and Chemokine Secretion from BEAS-2B Cells. *Pharmacology & Pharmacy* 2012; 3(2): 166–177.
37. Banerjee A and Gerondakis S. Coordinating TLR-activated signaling pathways in cells of the immune system. *Immunol Cell Biol* 2007; 85(6): 420–424.
38. Aksoy MO, Yang Y, Ji R, et al. CXCR3 surface expression in human airway epithelial cells: cell cycle dependence and effect on cell proliferation. *Am J Physiol Lung Cell Mol Physiol* 2006; 290(5): L909–L918.
39. Juliana C, Fernandes-Alnemri T, Kang S, Farias A, et al. Non-transcriptional priming and deubiquitination regulate NLRP3 inflammasome activation. *J Biol Chem* 2012; 287(43): 36617–36622.
40. Schroder K, Sagulenko V, Zamoshnikova A, et al. Acute lipopolysaccharide priming boosts inflammasome activation independently of inflammasome sensor induction. *Immunobiology* 2012; 217(12): 1325–1329.

41. Hetz C. The unfolded protein response: controlling cell fate decisions under ER stress and beyond. *Nat Rev Mol Cell Biol* 2012; 13(2): 89–102.
42. Bauernfeind FG, Horvath G, Stutz A, et al. Cutting Edge: NF- $\kappa$ B Activating Pattern Recognition and Cytokine Receptors License NLRP3 Inflammasome Activation by Regulating NLRP3 Expression. *The J Immunol* 2009; 183(2): 787–791.
43. O'Brien KM and Nonnenmann MW. Airborne Influenza A Is Detected in the Personal Breathing Zone of Swine Veterinarians. *PloS ONE* 2016; 11(2): e0149083.
44. Wilson RH, Maruoka S, Whitehead GS, et al. The Toll-like receptor 5 ligand flagellin promotes asthma by priming allergic responses to indoor allergens. *Nat Med* 2012; 18(11): 1705–1710.